Efficiency of a grazing-incidence off-plane grating in the soft-x-ray region

J. F. Seely, L. I. Goray, Benjawan Kjornrattanawanich, J. M. Laming, G. E. Holland, K. A. Flanagan, R. K. Heilmann, C.-H. Chang, M. L. Schattenburg, and A. P. Rasmussen

Efficiency measurements of a grazing-incidence diffraction grating in the off-plane mount were performed using polarized synchrotron radiation. The grating had 5000 grooves/mm, an effective blaze angle of 14°, and was gold coated. The efficiencies in the two polarization orientations (TM and TE) were measured in the 1.5–5.0 nm wavelength range and were compared with the efficiencies calculated using the PCGrate-SX code. The TM and TE efficiencies differ, offering the possibility of performing unique science studies of astrophysical, solar, and laboratory sources by exploiting the polarization sensitivity of the off-plane grating.   © 2006 Optical Society of America

OCIS codes: 050.1950, 050.1960, 300.6560.

1. Introduction

To achieve the science objectives for planned astrophysical and other missions, high spectral resolution and instrument sensitivity are required in the soft-x-ray wavelength range (1–20 nm). This can be achieved only by grazing-incidence diffraction gratings. Although the in-plane (classical) grating mount has traditionally been considered for future missions, with the grating grooves perpendicular to the incident beam, it has been suggested that the off-plane (conical) grating mount can provide superior performance. The choice of grating mount (in-plane or off-plane) depends on the ability to reliably design, produce, and replicate optimized gratings with high diffraction efficiencies. The accurate experimental measurement of the efficiencies of test gratings and the validation of efficiency simulation codes are essential to this process.

Compared with gratings in the classical in-plane mount, gratings in the off-plane mount have the potential for superior resolution and efficiency.[1–5] Grazing-incidence off-plane gratings have been suggested for the Constellation-X mission.[6]

The absolute efficiencies in higher orders in grazing off-plane diffraction geometries may reach very high values comparable to those obtained in the first order, which permits use of the high orders in the shortest-wavelength part of the operating range to the maximum extent possible.[7] In addition, efficiency calculations indicate that off-plane gratings, when properly oriented, can provide polarization sensitivity.[7] The polarization measurements can provide unique information about astrophysical sources not possible with existing instruments such as the XMM-Newton Reflection Grating Spectrometer and Chandra.

Off-plane grating efficiencies were first measured by Werner[8] using an electron-bombarded anode at four discrete wavelengths in the 0.83–4.45 nm range. At the U.S. Naval Research Laboratory (NRL), Neviere *et al.* measured off-plane and in-plane efficiencies in the 20–110 nm wavelength range.[9]

Off-plane grating measurements using an electron-bombarded x-ray source were carried out in association with a rocket spectrometer mission by Cash and co-workers[5,10,11] More recently, measurements of test gratings were performed by McEntaffer *et al.*[12,13]

J. F. Seely (john.seely@nrl.navy.mil) and J. M. Laming are with the Space Science Division, U.S. Naval Research Laboratory, Washington, D.C. 20375. L. I. Goray is with the International Intellectual Group, Incorporated, P.O. Box 335, Penfield, New York 14526. B. Kjornrattanawanich is with the Universities Space Research Association, National Synchrotron Light Source, Beamline X24C, Brookhaven National Laboratory, Upton, New York 11973. G. E. Holland is with SFA Incorporated, 2200 Defense Highway, Suite 405, Crofton, Maryland 21114. K. A. Flanagan, R. K. Heilmann, C.-H. Chang, and M. L. Schattenburg are with the Kavli Institute for Astrophysics and Space Research, Massachusetts Institute of Technology, Cambridge, Massachusetts 02139. A. P. Rasmussen is with the Columbia Astrophysical Laboratory, 550 West 120th Street, New York, New York 10027.

in association with plans for the Constellation-X mission.

Measurements of a test grating, fabricated on a silicon wafer at the MIT Space Nanotechnology Laboratory, were performed at four discrete wavelengths in the 0.99–4.48 nm range.[14] Measurements of several MIT test gratings were performed in off-plane and in-plane mounts using the Advanced Light Source synchrotron, in one polarization orientation, by Rasmussen *et al.*[15]

We report here the first detailed calibration of an off-plane grating using polarized synchrotron radiation in the two polarization orientations (TM and TE). The measured efficiencies are compared with the efficiencies calculated by the PCGrate-SX code in the two polarizations and using realistic groove profiles derived from atomic force microscope (AFM) measurements of the grating.

2. Conical Diffraction Pattern

The 5000 groove/mm master grating was fabricated at the MIT Space Nanotechnology Laboratory. The grating pattern was recorded holographically in resist on a bias-cut silicon wafer, and the wafer was anisotropically etched.[14] Replica gratings were produced by nanoimprint lithography and were coated with 5 nm of titanium and 20 nm of gold.[16] Scanning electron microscope images of the groove facets indicated a blazed groove profile and low microroughness. The design blaze angle was 7.5°, but as discussed below the efficiency measurements and the PCGrate-SX code calculations, using the groove profile derived from AFM, indicate that the effective blaze angle after coating was approximately 13°–15°.

The efficiency calibrations were performed at the NRL beamline X24C at the National Synchrotron Light Source. The beamline's monochromator provided dispersed radiation to a large calibration chamber that is a distance of 15 m from the monochromator and 30 m from the synchrotron. The synchrotron radiation from the bending magnet is polarized with the electric vector in the plane of the storage ring. The X24C beamline optics, operating at grazing angles in the x-ray and extreme-ultraviolet wavelength regions, preserve the polarization. Thus the beam delivered to the calibration chamber has the electric vector primarily in the horizontal direction. The beam polarization measured in the 10–30 nm range is 80%–90%, and the polarization is expected to be the same at shorter wavelengths.

The grating was mounted in the off-plane orientation as shown schematically in Fig. 1. The grating wafer was mounted by a three-point support on a goniometer platform with the grooves parallel to the incident radiation. The goniometer platform could be rotated by computer control about two orthogonal axes in the horizontal plane to precisely adjust the incidence angle (θ), with respect to the normal to the grating surface, and the azimuthal angle (ϕ) about the incident radiation beam. The goniometer was mounted on a support plate with x and y motions to accurately position the grating in the radiation beam.
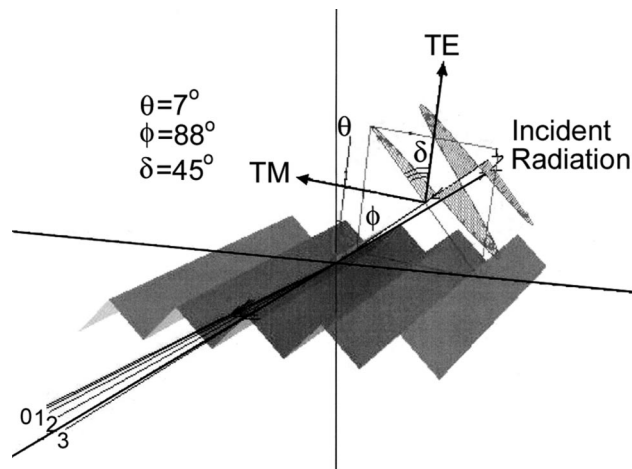

Fig. 1. Schematic of the off-plane grating and the conical diffraction pattern.

The support plate could also be rotated in a yaw angle about an axis perpendicular to the goniometer base and at the center of the grating, thereby varying the alignment of the grooves with the incident radiation beam. Finally, the support plate (and goniometer) could be rotated by 90° about the incident radiation beam to the TE ($\delta = 0°$) or TM ($\delta = 90°$) polarization orientations. Thus the grating had four rotational and two translational degrees of freedom.

The conical diffraction pattern was recorded by a phosphor- (Gd_2O_2S:Eu-) coated complementary metal-oxide semiconductor (CMOS) imager with 50.8 mm square active area and 48 μm pixels. The CMOS imager was mounted on a support fixture with four computer-controlled motions: x, y, rotation about the vertical axis, and pitch about the horizontal axis. The large area of the CMOS imager provided the ability to capture the entire conical diffraction pattern as shown in Fig. 2. The CMOS imager is controlled by a USB interface to a notebook computer, and the exposure and image download times are typically 10 s. Thus one can quickly recognize the diffraction features and move to the desired grating angles and incident wavelengths in practically real time.

The imager is composed of two 50.8 mm × 25.4 mm CMOS chips in close proximity. The faint horizontal artifact at the center of the image in Fig. 2 is the small gap between the two chips. The other two horizontal artifacts are two rows of insensitive pixels used for reading out the chips. These artifacts can easily be removed in software (not done in Fig. 2) and in practice do not significantly obscure the diffraction features. In addition, the artifacts are greatly reduced, and the signal-to-noise ratio is increased, when the CMOS imager is cooled with liquid nitrogen via a copper strap (the CMOS imager was not cooled for this grating calibration).

While the grating motions are accurately calibrated, we performed metrology on the conical diffraction pattern to confirm the expected changes when the grating is moved or the incident wavelength is altered. This is illustrated by the small subimages
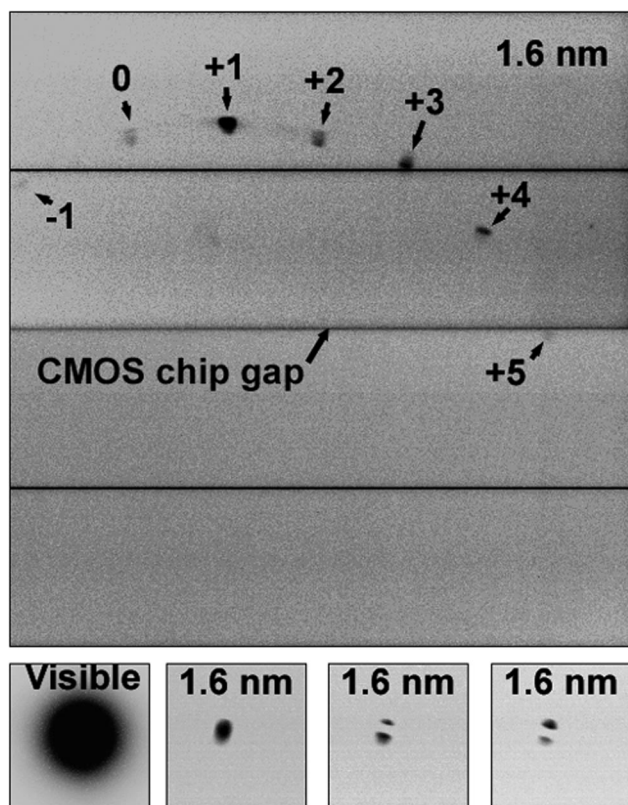
Fig. 2. CMOS image of the conical diffraction pattern for a wavelength of 1.6 nm. Shown below the CMOS image are subimages of the visible light beam and the 1.6 nm beam. The two subimages of the shadow of the grating in the 1.6 nm beam, shown at the lower right, illustrate how rapid feedback from the CMOS images can be used to establish grating alignment under x-ray illumination.

at the bottom of Fig. 2. From left to right, the four subimages are of the visible light beam from the monochromator (the zero diffraction order of the monochromator gratings attenuated by a sapphire window) when the test grating was withdrawn from the beam, the 1.6 nm wavelength beam when the grating was withdrawn and the 1.6 nm beam when the grating had been moved into the beam at two positions separated by 211 μm in the direction perpendicular to the beam. In practice, the visible light beam travels the same path as the dispersed beam and can be used to visually set up the grating and imager geometry before the calibration vacuum chamber is pumped. The shadow of the grating's silicon wafer substrate is seen in the last two subimages (1.6 nm beam), and the grating's roll angle about the beam is also apparent in the shadow.

In most cases, the grating angles were selected to correspond to an off-plane configuration proposed for the Constellation-X mission. The grating was positioned at a grazing angle of 1.73° ($\phi = 88.27°$) or 2.00° ($\phi = 88.00°$) and the grating was yawed by an angle of 1.0°, so the blazed groove facets slightly faced the incident beam. Referring to the grating equation for conical diffraction, $\sin \alpha + \sin \beta = m\lambda/d \sin \gamma$,[1,8,17,18] for a 1.73° grazing angle the

diffraction cone angle is $\gamma = 2.0°$ and the incidence angle with respect to the grating normal is $\alpha = 30.0°$. The +1 order was closest to being on blaze and appeared near the top ($\beta = 0$) of the diffraction cone as illustrated in Fig. 2. The on-blaze condition is that the angles of incidence and diffraction from the grating facets are equal (specular reflection), and then $\alpha + \beta = 2\varepsilon$ where ε is the blaze angle.

A 0.5 mm aperture defined the size and position of the beam that was incident on the grating. The aperture ensured that the beam illuminated a fixed area on the grating. The 0.5 mm beam underfilled the 5 cm grating grooved area at a typical grazing angle of 1.73°.

When measuring grating performance at a small grazing angle, the grating position and angular orientation, and the incident radiation beam position and divergence, must be precisely controlled and must be stable. In particular, when the radiation beam is scanned in wavelength, the movement of the beam on the grating and the detector must be small relative to the grating and the detector size. In our case, the size of the dispersed beam on the CMOS imager, positioned 80 cm from the grating and 120 cm from the 0.5 mm aperture, was typically 2 mm (42 pixels). Thus the dispersed beam's half-angle divergence from the 0.5 mm aperture was 0.036°. The beam movement in the CMOS images when the incident wavelength was scanned by the monochromator was measured to be up to four pixels, corresponding to a 0.009° angular shift from the 0.5 mm aperture. The pixel shift is small compared to the pixel separation between the orders (160 pixels at a 1.6 nm wavelength and greater at longer wavelengths). The pixel shift is predictable and could be removed from the data. In any case, the stability of the beam, which is critically important for the calibration of grazing-incidence optics, was well within the beam divergence and was typically <3% of the diffraction spot separation. This permitted precision metrology of the conical diffraction pattern in the CMOS images.

By illuminating the test grating with the zero order of the monochromator gratings and inserting thin metal filters in the beam, it was possible to illuminate the test grating with broadband radiation. Figure 3 shows portions of CMOS images for the case of two broad bands of radiation, provided by the monochromator's filtered zero order, and three discrete wavelengths (2.1, 3.0, and 5.0 nm) dispersed by the monochromator's first order. The lower wavelength limit of the two bandpasses (2 nm) was established by the selected monochromator grazing angle (5.4°). The upper wavelength limits were determined by the beam filtration. Numerous thin metal filters are mounted on two translation vacuum feedthroughs at the X24C beamline, and one or two selected filters can be easily moved into the beam. The 2–7 nm bandpass was established by a 158 nm thick aluminum filter (the wavelengths transmitted by the filter longer than the aluminum L edge at 17 nm were dispersed beyond the field of view
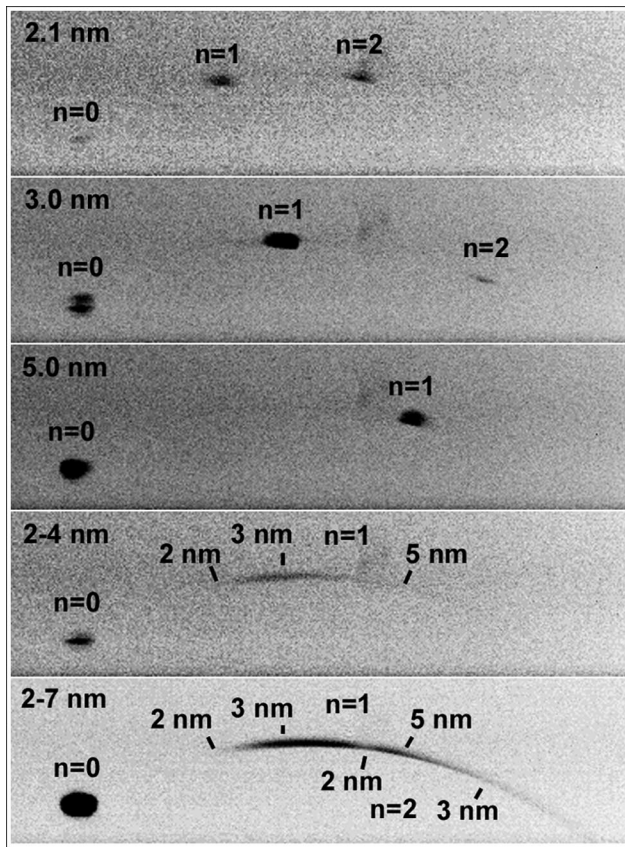
Fig. 3. CMOS images of the conical diffraction pattern for illumination by monochromatic radiation with wavelengths of 2.1, 3.0, and 5.0 nm and by broadband radiation of 2–4 and 2–7 nm.

Fig. 4. The measured zero-order TM efficiency for $\phi = 88.00°$.

of the CMOS imager). The 2–4 nm bandpass was established by a 200 nm thick nickel filter in combination with the aluminum filter.

Figure 3 illustrates the ability to easily illuminate the test grating with selected monochromatic radiation or bright broadband radiation. This simulates the two extreme cases when a spectrometer containing the off-plane grating is illuminated by a radiation source with primarily spectral line emission or continuum emission. In addition, when illuminated by monochromatic radiation at the X24C beamline, the absence of continuum dispersed between the orders permits the study of monochromatic radiation scattered from the grating facets. These are critically important measurements for the test gratings that can determine the ability to carry out the science objectives of an astrophysical or solar mission.

3. Efficiency Measurements

Although the CMOS images provided snapshots of the entire conical diffraction pattern and could be used to derive the efficiencies, a more accurate technique is to use absolutely calibrated silicon photodiodes with a known linear response over many decades and low noise. The photodiodes were of two types, AXUV-100 with a 10 mm × 10 mm active area and AXUV-96 with a 6 mm × 16 mm area, both from International Radiation Detectors Inc. Three photo-
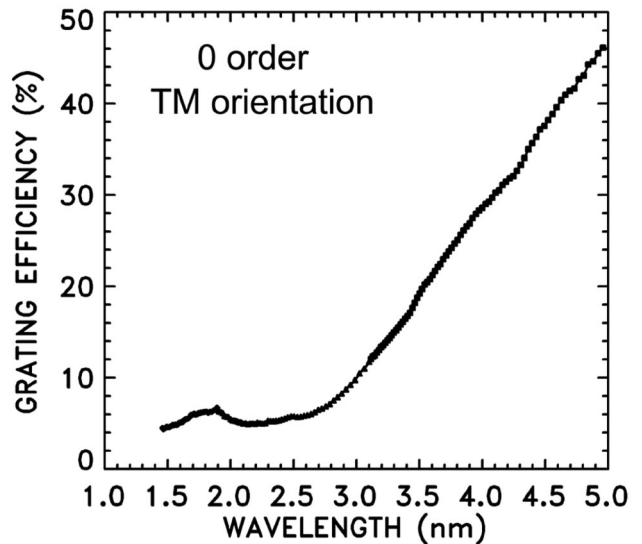
diodes were mounted on the same support fixture as the CMOS imager and could be moved into the radiation beam under computer control. The three photodiodes had the following apertures: 6.4 mm round (photodiode type AXUV-100), 9.6 mm round (AXUV-100), and 3 mm × 16 mm rectangular (AXUV-96). On the basis of the positions of the dispersed orders in the CMOS image, a selected photodiode could be accurately moved to the dispersed orders for the measurement of the absolute intensity. An additional photodiode was mounted between the grating and the 0.5 mm aperture for the purpose of measuring the direct beam without having to move the grating from the beam. The beam underfilled all the photodiode apertures, and the photodiodes were cross calibrated.

Since the zero-order beam diffracted from the test grating does not move in angle when the incident wavelength is scanned, it was possible to position a photodiode in the zero order and scan the wavelength in small steps (0.01 nm) while recording the photodiode current at each step. Small wavelength steps are necessary to observe polarization anomalies that were predicted (by PCGrate-SX calculations[7]) to occur primarily in the TM orientation. The absolute zero-order efficiency was derived by dividing by the direct beam current. The resulting zero-order efficiency is shown in Fig. 4, and no efficiency jumps resulting from TM polarization anomalies were observed.

The 3 mm × 16 mm aperture was sufficiently tall to intercept a number of diffracted orders near the top of the diffraction cone when scanned horizontally across the diffraction pattern under computer control. The efficiencies in the dispersed orders were normalized by the zero-order absolute efficiency measured by the silicon photodiode (Fig. 4). Shown in Fig. 5 are the 0- and +1-order TM efficiencies when the wavelength was stepped from 3.0 to 5.1 nm in 0.1 nm increments. The change in the horizontal po-
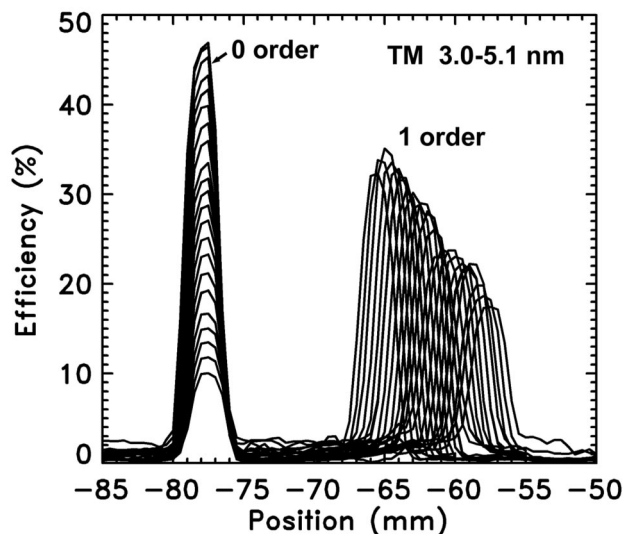
Fig. 5. Detector scans through the 0 and +1 orders for 3.0–5.1 nm incident wavelengths and $\phi = 88.00°$.

sition of the +1 order is consistent with the grating equation that predicts a horizontal change by $m\lambda/d$.[1]

Shown in Fig. 6 are the TM efficiencies of the 0, +1, and +2 orders measured by positioning the 6.4 mm apertured photodiode in the orders. Small features appear near the K edges of O (2.28 nm) and N (3.10 nm) resulting from slightly different thin films on the surfaces of the two photodiodes used for the measurements (the SiO_2 photodiode surfaces are nitrided for radiation hardness).

The efficiencies measured in the TE grating orientation, recorded prior to the TM measurements, are not as complete as the TM data because prominent polarization anomalies were not predicted to occur in the TE orientation. In addition, the CMOS imager and the photodiode detectors were positioned closer to the grating during the TE measurements, and this af-
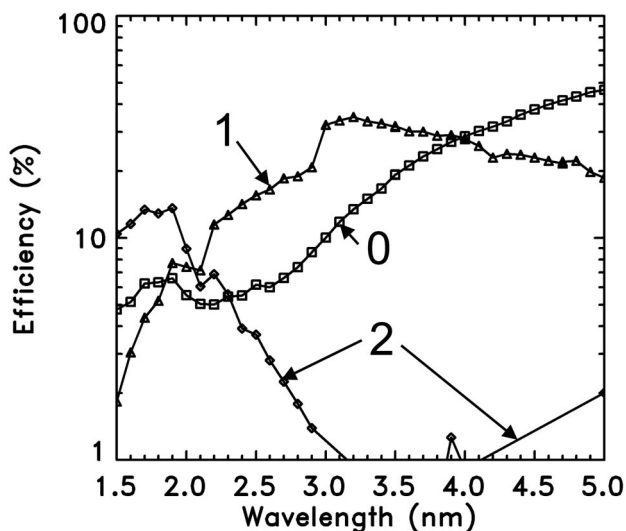

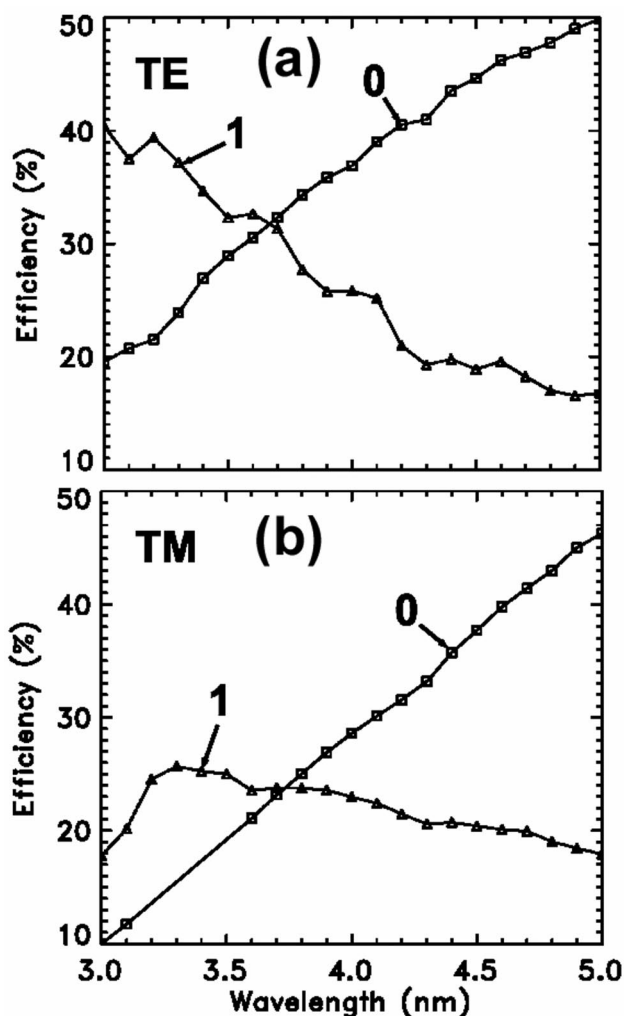Fig. 7. Measured zero- and first-order efficiencies in the (a) TE orientation with $\phi = 88.00°$ and (b) TM orientation with $\phi = 88.27°$.

fected the quality of the short-wavelength (<3 nm) data where the diffracted orders were not well separated. However, the diffracted orders were well separated at the longer wavelengths (>3 nm), and the measured TE efficiencies in the 0 and +1 orders are shown in Fig. 7 along with the TM efficiencies for comparison. The efficiencies measured in the TE and TM orientation significantly differ, and this indicates that the grating has polarization sensitivity when in the off-plane mount.

4. Efficiency Calculations

The measured TM and TE efficiencies were compared with the efficiencies calculated by the PCGrate-SX code developed by Goray.[7] For the case of normal-incidence gratings with opaque coatings (e.g., gold or aluminum) and multilayer interference coatings, this code has been validated by detailed comparisons with efficiencies measured using synchrotron radiation (Refs. 19 and 20 and references therein). PCGrate-SX was recently used to design and fabricate the

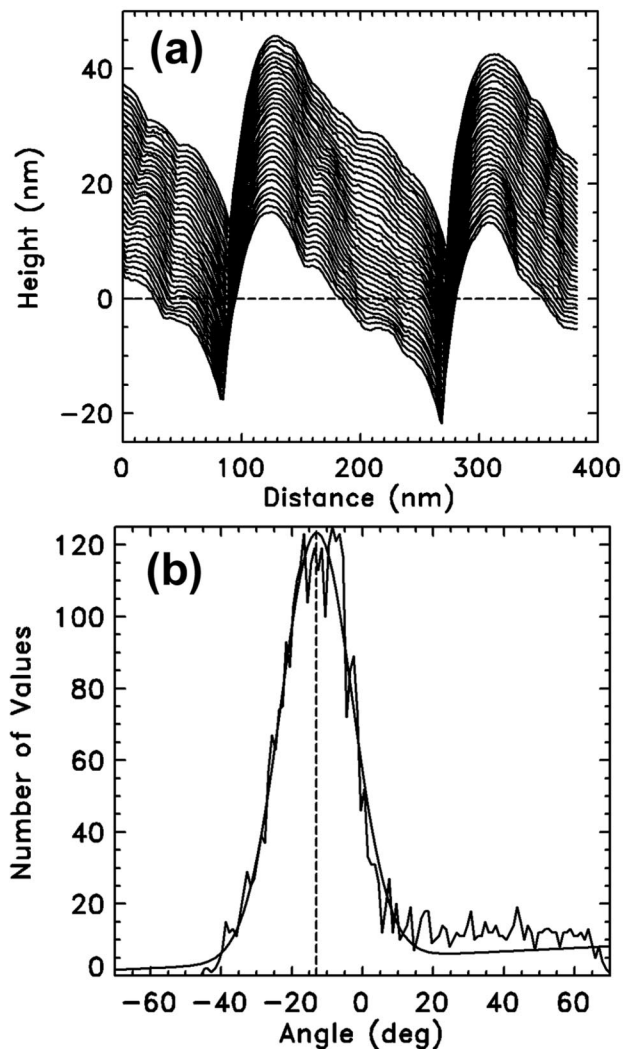Fig. 6. Measured TM efficiencies in the 0, 1, and 2 orders and for $\phi = 88.00°$.

Fig. 8. (a) AFM scans across the grooves near the center of the grating. (b) Histogram of the angles of pairs of points on the AFM scans giving a measure of the average blaze angle.

Fig. 9. Calculated (solid curves) and measured (dashed curves) efficiencies in the (a) TE and (b) TM grating orientations.

multilayer-coated grating for the Extreme Ultraviolet Imaging Spectrometer for the Solar-B mission.[20]

Initial comparisons indicated that the efficiencies calculated assuming a 7.5° blaze angle, the value expected from the grating fabrication process, were in fundamental disagreement with the measured efficiencies. This can be seen by calculating the on-blaze wavelength: $\lambda = 2d \sin \varepsilon \sin \sigma$, where the assumed blaze angle is $\varepsilon = 7.5°$ and the grazing angle on the grating facets is $\sigma = 1.75°$ (differing slightly from the grazing angle of 1.73° with respect to the grating surface). The calculated on-blaze wavelength is $\lambda = 1.6$ nm, while the observed TM +1-order efficiency peaks at 3.3 nm (Fig. 6) implying a 15° blaze angle.

An AFM study of the grooved area confirmed the larger than expected blaze angle. The AFM scans across the grooves near the center of the grating are shown in Fig. 8(a), where each scan is displaced vertically by 1 nm for ease of viewing. The standard
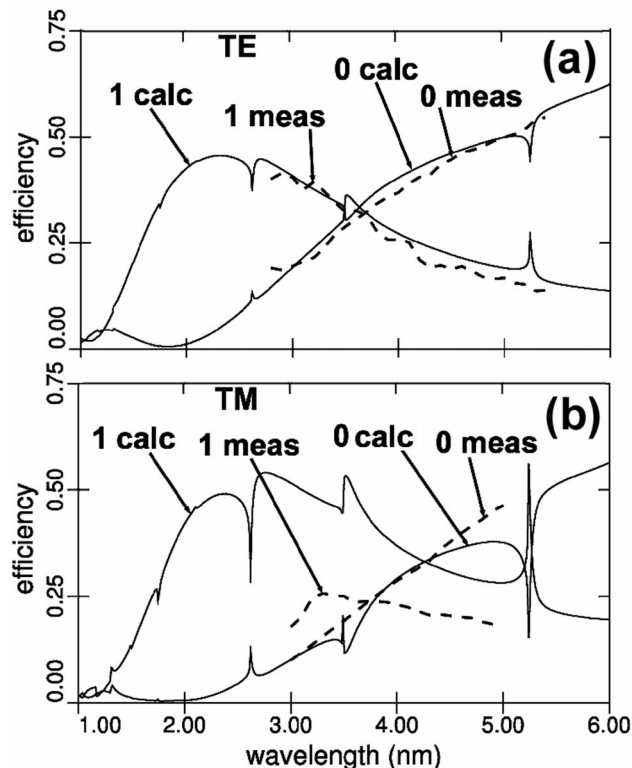
deviation of the data points from the average scan curve is 0.89 nm and is a measure of the microroughness of the groove profile. The histogram of the angles between each pair of scan points is shown in Fig. 8(b), where a Gaussian curve is fitted to the angle distribution. The top corners of the groove profiles are rounded, and this results in a rather broad distribution of angles with a centroid value of 13°. The average values of the blaze angles measured at seven points distributed on the grooved area ranged from 8.9° to 15°, and the microroughness values ranged from 0.66 to 0.92 nm. Thus there was considerable variation of the grooves over the 5 cm patterned area. AFM data that were taken before the titanium and gold coating of the imprinted grating showed microroughness of approximately 0.2 nm (Ref. 16) and blaze angles of around 8°, which indicate that deposition of the metal films onto the polymer-based imprint resist led to the observed changes in groove profile.

PCGrate-SX calculations were initially performed using a representative groove profile from the AFM image shown in Fig. 8 and with 1.0 nm microroughness. The incident beam was assumed to be 80% polarized. The efficiencies calculated for the grating in the TE and TM orientations are shown by the solid curves in Fig. 9. A sharp spike (or jump) in efficiency occurs when the diffraction angle of an order, measured from the grating normal, exceeds 90°. Thus, as the wavelength increases, efficiency jumps in the lower orders occur when higher orders are diffracted
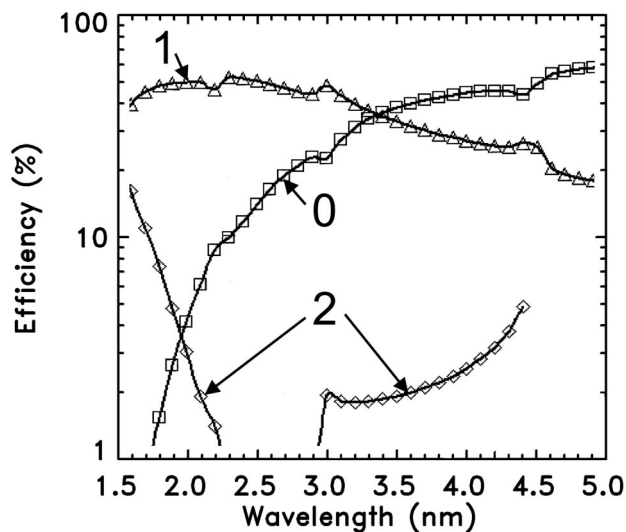
Fig. 10. Calculated TM efficiencies for an assumed groove profile with a 36.2 nm depth and 0.5 nm microroughness.

into the grating surface and become evanescent. The efficiency jumps are deeper in the TM orientation where the electric vector of the diffracted wave is approximately parallel to the surface of the grating (see Fig. 1 for $\delta = 90°$).

Shown by the dashed curves in Fig. 9 are the measured efficiencies from Fig. 7. As seen in Fig. 9(a), the calculated and measured TE efficiencies are in good overall agreement, except that the small anomalous jumps in efficiency were not observed. Large differences between the calculated and measured TM efficiencies occur in Fig. 9(b), including the absence of the predicted large anomalous jumps in efficiency. The measurement of the TM zero-order efficiency with small wavelength steps (0.01 nm) shown in Fig. 4 conclusively indicates that efficiency jumps are not observed. Other comparisons indicated that the measured TM second order, and the measured ratio of the two-to-one orders, significantly disagree with the calculations.

There are several possible explanations for the disagreements between the calculated and measured efficiencies. First, the AFM images indicate that the groove profile varies over the grooved area, and the calculated efficiencies differ significantly when different groove profiles are assumed. Second, the incident beam is not purely (100%) polarized, and this somewhat reduces the ability to observe strong polarization effects in the TM orientation. Finally, the microroughness along the grooves was not measured by AFM scans along the grooves, and incorrect assumed microroughness may affect the calculated efficiencies.

To illustrate the sensitivity of the calculated efficiencies to small changes in the assumed groove profile, Fig. 10 shows the TM efficiencies calculated assuming a 36.2 nm groove depth (rather than the 24.8 nm depth for the calculations shown in Fig. 9) and 0.5 nm microroughness. Efficiency jumps are ab-

sent, and the calculated efficiencies shown in Fig. 10 are in qualitative agreement with the measured TM efficiencies shown in Fig. 6, although the absolute values of the calculated and measured efficiencies differ.

5. Discussion

The absolute efficiency of a 5000 groove/mm grating in the off-plane mount was measured in the TM and TE orientations using polarized synchrotron radiation. The measured efficiencies were compared with the efficiencies calculated using the PCGrate-SX code. The efficiency jumps predicted by code calculations were not observed, presumably because of the variation of the groove profile over the area illuminated by the grazing-incidence radiation beam. The calculated and measured TE absolute efficiency values were in good agreement, while significant differences occurred for the TM values. Further experimental and computational studies are necessary to identify the cause of the TM differences, including more detailed AFM characterizations of the shape and microroughness of the groove profile across the grating area. Also, the calculation model should be improved to more accurately predict TM efficiencies with anomalies.

For a given wavelength, the measured first-order TE and TM efficiencies differ, and the off-plane grating therefore has polarization sensitivity. This can be exploited to measure the polarization of radiation from astrophysical, solar, and laboratory sources in the soft-x-ray region.

References

1. W. Cash, "Echelle spectrographs at grazing incidence," Appl. Opt. **21,** 710–717 (1982).
2. M. C. Hettrick and S. Bowyer, "Variable line-space gratings: new designs for use in grazing incidence spectrometers," Appl. Opt. **22,** 3921–3924 (1983).
3. W. Cash, "X-ray spectrographs using radial groove gratings," Appl. Opt. **22,** 3971–3976 (1983).
4. M. C. Hettrick, "Aberrations of variable line-space gazing incidence gratings in converging light beams," Appl. Opt. **23,** 3221–3235 (1984).
5. W. C. Cash, "X-ray optics. 2: A technique for high resolution spectroscopy," Appl. Opt. **30,** 1749–1759 (1991).
6. R. McEntaffer, W. Cash, and A. Shipley, "Off-plane gratings for Constellation-X," in Proc. SPIE **4851,** 549–556 (2002).
7. L. I. Goray, "Rigorous efficiency calculations for blazed gratings working in in- and off-plane mountings in the 5–50-Å wavelength range," in Proc. SPIE **5168,** 260–270 (2004).
8. W. Werner, "X-ray efficiencies of blazed gratings in extreme off-plane mountings," Appl. Opt. **16,** 2078–2080 (1977).
9. M. Neviere, D. Maystre, and W. R. Hunter, "On the use of classical and conical diffraction mountings for XUV gratings," J. Opt. Soc. Am. **68,** 1106–1113 (1978).
10. D. Windt and W. Cash, "Laboratory evaluation of conical diffraction spectrographs," in Proc. SPIE **503,** 98–105 (1984).

11. E. Wilkinson, J. C. Green, and W. Cash, "The extreme ultraviolet spectrograph: a radial groove grating, sounding rocket-borne, astrophysical instrument," Astrophys. J. Suppl. **89,** 211–220 (1993).

12. R. McEntaffer, S. Osterman, W. Cash, J. Gilchrist, J. Flamand, B. Touzet, F. Bonnemason, and C. Brach, "X-ray performance of gratings in the extreme off-plane mount," in Proc. SPIE **5168,** 492–498 (2004).

13. R. McEntaffer, F. Hearty, B. Gleeson, and W. Cash, "An x-ray test facility for diffraction gratings," in Proc. SPIE **5168,** 499–507 (2004).

14. R. K. Heilmann, M. Akilian, C.-H. Chang, C. Chen, C. Forest, C. Joo, P. Konkola, J. Montoya, Y. Sun, J. You, and M. L. Schattenburg, "Advances in reflection grating technology for Constellation-X," in Proc. SPIE **5168,** 271–282 (2004).

15. A. Rasmussen, A. Aquila, J. Bookbinder, C.-H. Chang, E. Gullikson, R. K. Heilmann, S. Kahn, F. Paerels, and M. L. Schattenburg, "Grating arrays for high-throughput soft x-ray spectrometers," in Proc. SPIE **5168,** 248–259 (2004).

16. C.-H. Chang, J. C. Montoya, M. Akilian, A. Lapsa, R. K. Heilmann, M. L. Schattenburg, M. Li, K. A. Flanagan, A. P. Rasmussen, J. Seely, J. Laming, B. Kjornrattanawanich, and L. I. Goray, "High fidelity blazed grating replication using nanoimprint lithography," J. Vac. Sci. Technol. B **22,** 3260–3264 (2004).

17. G. Spencer and M. Murty, "General ray-tracing procedure," J. Opt. Soc. Am. **52,** 672–678 (1962).

18. D. Maystre and R. Petit, "Principe d'un spectromètre à réseau à transmission constante," Opt. Commun. **5,** 35–37 (1972).

19. L. I. Goray and J. F. Seely, "Efficiencies of master, replica, and multilayer gratings for the soft x-ray–extreme-ultraviolet range: modeling based on the modified integral method and comparisons with measurements," Appl. Opt. **41,** 1434–1444 (2002).

20. J. Seely, C. Brown, D. Windt, S. Donguy, and B. Kjornrattanawanich, "Normal-incidence efficiencies of multilayer-coated laminar gratings for the extreme-ultraviolet imaging spectrometer on the Solar-B mission," Appl. Opt. **43,** 1463–1471 (2004).